

Tearing transition and plastic flow in superconducting thin films

M.-CARMEN MIGUEL¹ AND STEFANO ZAPPERI^{*2}

¹Departament de Física Fonamental, Facultat de Física, Universitat de Barcelona, Diagonal 647, E-08028, Barcelona, Spain

²INFN unità di Roma 1 and SMC, Dipartimento di Fisica, Università "La Sapienza", P.le A. Moro 2, 00185 Roma, Italy

*e-mail: zapperi@pil.phys.uniroma1.it

Published online: 22 June 2003; doi:10.1038/nmat909

A new class of artificial atoms, such as synthetic nanocrystals or vortices in superconductors, naturally self-assemble into ordered arrays. This property makes them applicable to the design of novel solids, and devices whose properties often depend on the response of such assemblies to the action of external forces. Here we study the transport properties of a vortex array in the Corbino disk geometry by numerical simulations. In response to an injected current in the superconductor, the global resistance associated to vortex motion exhibits sharp jumps at two threshold current values. The first corresponds to a tearing transition from rigid rotation to plastic flow, due to the reiterative nucleation around the disk centre of neutral dislocation pairs that unbind and glide across the entire disk. After the second jump, we observe a smoother plastic phase proceeding from the coherent glide of a larger number of dislocations arranged into radial grain boundaries.

The production of ordered self-assembled structures of various materials as diverse as synthetic nanocrystals, magnetic colloids, charged particles in Coulomb crystals, proteins and surfactants, or vortices in type II superconductors and in Bose–Einstein condensates, has attracted much interest for various fundamental and practical reasons, which are ultimately concerned with their collective properties (optical, magnetic, mechanical or transport properties)^{1–3}. In particular, much experimental and theoretical effort has been devoted to characterizing the phase diagram of type II superconductors⁴. Depending on the value of the magnetic field H , temperature T , and sample preparation, vortices can either form a crystal⁵, which at higher temperatures melts into a liquid^{6–9}, or, due to quenched disorder, they can be found in more complex phases, such as the vortex glass¹⁰, the Bose glass¹¹ or the Bragg glass^{12,13}. Of special importance is the non-equilibrium response of vortex matter to the flow of an external current^{14,15}, because the dissipative motion of the vortices induces an undesirable macroscopic resistance. The moving phase can be as simple as the collective motion of an elastically deforming vortex crystal, or can be more complex, such as in plastic¹⁶ or in channel vortex flow¹⁷.

Transport experiments in superconductors are often performed in a strip geometry: current is injected in one side and removed from the opposite side^{16,17}. The current–voltage (I – V) curve provides an indirect measure of vortex dynamics, because vortex motion induces an electric field proportional to the vortex velocities. It has been noticed that the sample boundary has an important effect on the moving vortex phase complicating the interpretation of the results^{18,19}; a problem that is overridden in the Corbino disk geometry^{15,19–23}. There, the current is applied at the disk centre and flows radially towards the boundary. Vortices tend to move in concentric circles without crossing the sample boundaries, avoiding edge contamination.

Vortices in the Corbino geometry experience a force gradient¹⁵, and thus exhibit intriguing dynamic phases as a function of T , H , and I . The vortex velocity profiles have been evaluated after measuring the voltage drop across a series of contacts placed radially on a $\text{YBa}_2\text{Cu}_3\text{O}_{7-\delta}$ disk²¹. For low currents and temperatures, all the vortices were found to move as a rigid solid, giving rise to a linear velocity profile $v(r) = \Omega r$, where r is the distance from the disk centre. Above a threshold current I_0 , the vortex crystal cannot sustain the shear stress induced by the resulting

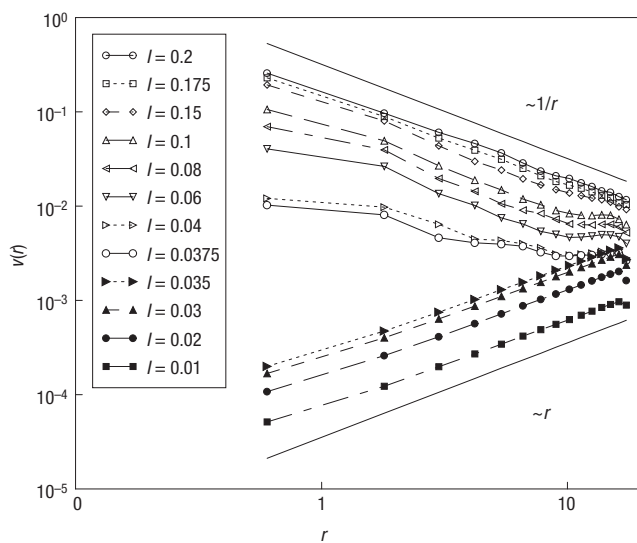


Figure 1 The velocity (v) profiles as a function of the applied current (I) for $N = 1032$ vortices in a disk of radius $D = 18$. For $I < I_0 = 0.036$ the profile is linear, corresponding to a rigid rotation of the lattice. For $I > I_0$ the profile deforms, indicating plastic flow. At high drives, the profile simply decays as $1/r$, where r is the distance from the disk centre.

inhomogeneous Lorentz force, and the response becomes plastic. Finally, above the vortex lattice melting temperature T_M , the velocity profile is fluid-like and decays as $v(r) \sim 1/r$. A theoretical model of vortex flow in the Corbino geometry has been analysed, and shows the shear yielding as a dislocation unbinding transition^{22,23}. Plastic flow would appear as soon as the current-induced shear stress is large enough to separate an existing pair of bound dislocations.

In this paper, we first study transport in the Corbino disk by $T = 0$ molecular dynamics (MD) simulations of interacting vortices^{24–26}. As in the experiments, for low currents we find a linear velocity profile that corresponds to the rigid rotation of the vortex lattice. Above a threshold current I_0 , the profile ceases to be linear, indicating the onset of plastic flow. Our simulations enable a close inspection of the lattice topology, which unveils the microscopic origin of this dynamic transition: at and above I_0 , new dislocation pairs are created, mainly within the highly strained central region, which readily unbind and glide along all possible crystalline directions giving rise to plastic flow. These processes occur repeatedly, yielding a strongly fluctuating voltage noise, which is reminiscent of the intermittent behaviour observed in plastically deforming crystals²⁷. For currents larger than a second threshold I_1 , we observe that voltage fluctuations decrease and vortices end up moving in uncorrelated annular channels, displaying a laminar $1/r$ velocity profile. In this regime, we find a larger amount of dislocations in the crystal, most of them forming radial grain boundaries that span the entire disk and glide in the tangential direction. The crystal reorientations associated with the presence of these grain boundaries make possible a steady regime of plastic deformation in the azimuthal direction. In addition, the exponential screening of shear stress produced by grain boundaries²⁸ enhances the number of nucleation events. The number of dislocations after the second jump at I_1 reaches a maximum value, corresponding to the presence of quite densely packed grain boundaries. We observe that the plastic deformation of the crystalline film proceeds with the glide motion of these grain boundaries.

We measured the plastic threshold current I_0 for different values of the disk radius D and vortex number N , and later show (in Fig. 5) that

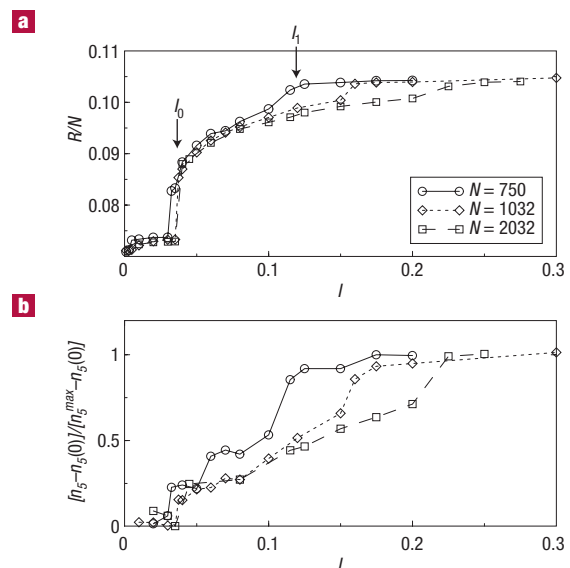


Figure 2 The resistance and the number of fivefold vortices as a function of the current. **a**, The normalized resistance R/N as a function of the applied current for N vortices in a disk of radius $D = 18$. **b**, The excursions in the average steady number of five-fold coordinated vortices n_5 for different N by plotting $[n_5 - n_5(0)]/[n_5^{\max} - n_5(0)]$. The arrows indicate I_0 and I_1 for $N = 750$.

the data collapse into a single curve when plotted against the crystal average lattice spacing a . As predicted previously²³, I_0 is proportional to the vortex crystal shear modulus c_{66} . Indeed, the curve follows very closely the dependence of c_{66} on the lattice spacing or field strength²⁹. A simple evaluation of the energy cost of a new dislocation pair provides a good quantitative estimate of this threshold current.

In the Corbino geometry, a disk-shaped superconductor is placed in a magnetic field parallel to the disk axis, and a current I is injected at a metal contact in the disk centre and removed at the disk boundary. Thus, the current density inside the disk is given by $\vec{j}(\vec{r}) = \hat{r}I/(2\pi rh)$, where h is the thickness of the specimen. This radial current generates an azimuthal Lorentz force acting on the vortices $\vec{f}_i(r) = \hat{\theta}\Phi_0 I(r)/c$, where Φ_0 is the quantized flux carried by the vortices, c is the speed of light, and $\hat{\theta}$ is the azimuthal versor. In addition, a pair of vortices interact with each other through a long-range force $\vec{f}_{vv}(\vec{r}) = AK_1(r/\lambda)\hat{r}$, where $A = \Phi_0^2/(8\pi^2\lambda^3)$, λ is the London penetration length, and K_1 is a Bessel function³⁰. Taking into account these interactions, we solve numerically the dynamics of N vortices confined in a disk of radius D (see the Methods section, describing the technical details of the simulations).

As in previous experiments²¹, we first measure azimuthal velocities v and compute the variation of the velocity profile $v(r)$ with I (see Fig. 1). At low currents, the velocity profile follows a linear law, $v(r) = \Omega r$ with angular velocity $\Omega \propto I$. This corresponds to a rigid rotation of the vortex crystal, as observed experimentally²¹. Above a threshold I_0 , the velocity profile starts to deform, with large tangential velocities in the centre, which then decay towards the boundary. At higher currents, the profile becomes smoother, decaying as $1/r$, characteristic of a laminar response.

To better identify the transitions in the system rheology, we measure the variations of the flow resistance $R \equiv \sum_i v_i/I$ with I . After an initial transient, the resistance reaches a statistically steady state, which fluctuates strongly in the plastic regime and is much smoother in the solid and laminar phases. Figure 2a shows the steady-state resistance for different values of N (at $D = 18$) as a function of I . We have normalized these curves by the corresponding number of vortices N to better

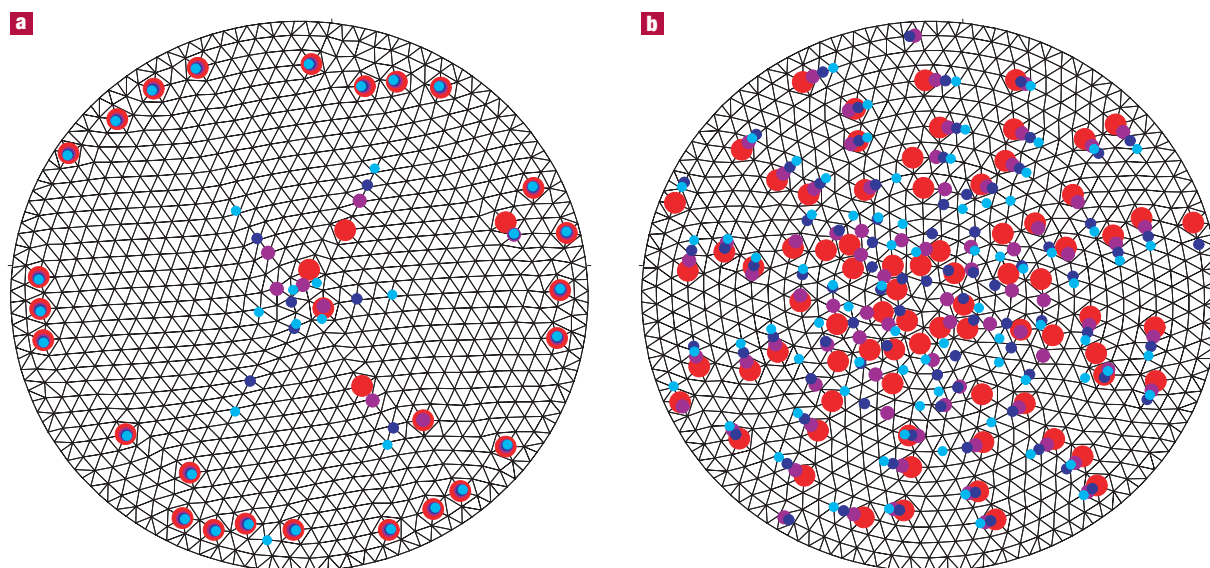


Figure 3 A series of snapshots illustrating dislocation dynamics. The system consists of $N = 1032$ vortices in a disk of radius $D = 18$ under two different applied currents: **a**, $I = 0.04$ and **b**, $I = 0.3$. Fivefold coordinated vortices are highlighted with coloured circles. Different colours correspond to four different time steps separated by an interval $\Delta t = 100$. Initially they are red, then violet, blue, and cyan. As a reference, on each plot we also show the Delaunay triangulation for the initial time step considered. Notice the radial motion of some defects in the plastic phase (**a**), and the tangential glide of grain boundaries (red circles oriented in the radial direction) in the laminar phase (**b**).

visualize their characteristic features. The curves show a first sharp jump around I_0 corresponding to the breakdown of the linear velocity profile, and a smaller jump at I_1 , indicating the onset of the hyperbolic profile. The final plateau scales with the number of moving vortices N . Indeed in this laminar regime, a scaling factor of N/D follows from a simple continuum approximation with a constant density of vortices. A direct inspection of the topology of the lattice allows the nature of the transitions to be clarified. We construct the Delaunay triangulation of the vortex positions in the disk to characterize their topology. Most of the vortices are sixfold, as in a perfect triangular lattice such as the Abrikosov lattice. A pair of fivefold and sevenfold neighbouring vortices identifies an edge dislocation in the lattice, a topological defect characterized by its Burgers vector²⁸ \vec{b} . Dislocations produce long-range stress and strain fields in the host crystal, experience the so-called Peach–Koehler force due to the local stress, and move mainly by gliding²⁸ along the direction of \vec{b} .

For $I < I_0$, all vortices within the bulk of the disk are sixfold whereas a large number of fivefold- and sevenfold-coordinated vortices are only observed along the boundary. These are geometrically necessary dislocations and disclinations, which need to be present in order to adjust a triangular lattice into a circular geometry. Like the resistance, the number of five/sevenfold coordinated vortices fluctuates around a steady average value after an initial transient. Figure 2b shows the behaviour of the average steady number of fivefold vortices n_5 as a function of the current. We have subtracted the average number of geometrically necessary boundary defects $n_5(0)$, and normalized the curves by its maximum value $n_5^{\max} - n_5(0)$ to better visualize their main features. The curves in Fig. 2b closely resemble the behaviour of the resistance in Fig. 2a, with jumps at I_0 and I_1 (see also Supplementary Information, Fig. S1 corresponding to a disk of radius $D = 36$). As the current overcomes I_0 , new defects start to nucleate near the centre of the lattice. Typically, we observe the reiterative formation of new dislocation dipoles (two dislocations with opposite Burgers vectors), that unbind and glide along the direction of their Burgers vector, in most cases towards the disk boundary (see Fig. 3a, and movies 1 and 2 in the

Supplementary Information). To accommodate the shear stress generated by the external current, the crystal should nucleate dislocations that are able to glide either radially or tangentially. Nevertheless, in the undistorted triangular lattice (or when the concentration of free dislocations is low), the dislocations that are nucleated are the most elementary, with Burgers vectors along the three basic crystalline directions. Of those, only the ones with \vec{b} almost parallel to the radial direction can easily glide over long distances due to the Peach–Koehler forces involved.

As time goes on, the dislocation flow process exhibits an erratic character, because dislocation pairs at short distances may annihilate each other or react to form a new dislocation; they assist the nucleation process at intermediate distances, and may even form various metastable structures. This intricate process is reflected by the strongly fluctuating flow resistance and the non-linear velocity profile. Figure 4 shows that at the onset of the plastic phase, the resistance noise power spectrum $S(\omega) = |\int dt R(t) e^{i\omega t}|^2$ (where ω is the frequency) displays a non-trivial power law decay $\omega^{-\beta}$ with $\beta = 1.5$. This is also apparent from the inset of Fig. 4, which displays the relative standard deviation of the resistance fluctuations as a function of current. We can then conclude that in the Corbino disk, strong voltage noise is a fingerprint of the onset of plastic deformation in the lattice.

Further increase of the current beyond $I = I_1$ results in a smoother flow, with most vortices moving in uncorrelated concentric trajectories. Here, dislocation flow appears to be quite peculiar because a significant number are settled in walls (grain boundaries) oriented along the radial direction, which tend to glide coherently in the azimuthal direction. Grain boundaries produce the necessary deformations of the crystal that allow a stationary tangential flow (see Fig. 3b and movies 3 and 4 in the Supplementary Information). Besides, the long-range stress field generated by free dislocations is screened out with their arrangement into grain boundaries. The screening length grows with the average distance separating contiguous dislocations in the wall, that is, the grain-boundary spacing. In a close-packed grain boundary, the spacing is of the order of a few crystal lattice constants a , and consequently,

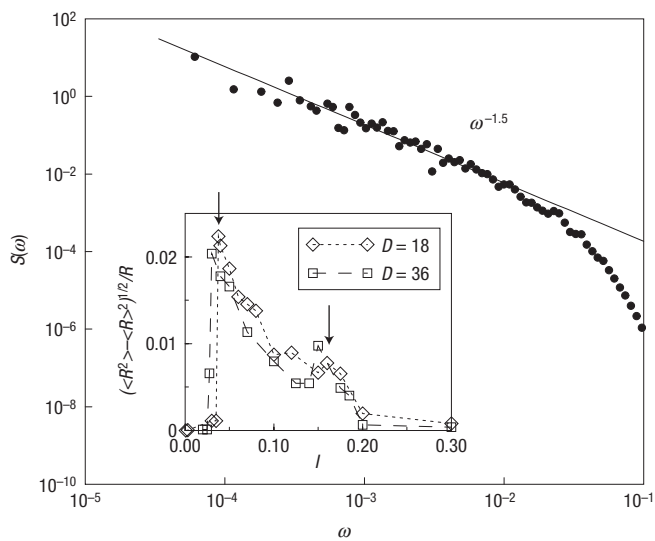


Figure 4 The resistance noise power spectrum for $N = 1032$ vortices in a disk of radius $D = 18$ under an applied current $I = 0.0375$. $S(\omega)$ is defined in the text. There is a region of power law decay well fit by $\omega^{-1.5}$. The inset shows the relative resistance noise standard deviation as a function of the current for $D = 18$ and $D = 36$. The peaks (arrowed) correspond to the transitions from solid to plastic and from plastic to laminar.

the number of dislocations in a radial grain boundary of size D grows as D/a . We indeed observe that the asymptotic number of dislocations in the laminar regime grows as $n_5^{\max} \propto D/a \propto N^{1/2}$ (see Supplementary Information, Fig. S2). We also observe that relative fluctuations of dislocation number and resistance (see inset in Fig. 4) are consequently reduced in this regime. Thus at and above I_0 , the rate of nucleation of new dislocations is big enough to ensure the formation and maintenance of these type of grain boundaries whose cooperative motion marks the new regime of plastic deformation.

Motivated by the observation that the onset of plasticity corresponds to the reiterative nucleation of topological defects around the centre of the disk, we estimate I_0 by computing the energy cost of a dislocation dipole²³. Very much like in any other ordinary crystal, the energy cost of an edge dislocation in the vortex lattice is made up of two contributions: the core energy F_c and the elastic energy F_e . The elastic energy cost F_e is proportional to the shear modulus of the crystal, and grows with the logarithm of the system size²⁸ D . The order of magnitude of the core energy per unit length can be estimated using the same variational argument that has been proposed³¹ for a vortex line in the xy -model. It turns out that F_c is proportional to $c_{66} b^2 / 4\pi$ for each dislocation, where c_{66} is the local shear modulus of the vortex lattice.

The elastic energy cost of a new dislocation dipole, such as the ones observed in the plastic phase, is independent of the system size and grows with the relative distance between the dislocations r_d —which, right at the moment of the creation event, is of the order of the lattice spacing—as $b^2 c_{66} / (2\pi) \ln(r_d/r_c)$, where r_c is a variational short-distance cutoff. Because both r_d and r_c are of the order of the lattice spacing, the core energy of the new dislocation dipole $2F_c$ is the leading energetic contribution for the proliferation of new pairs. The inhomogeneous elastic shear stress and strain induced by the external current in the Corbino disk geometry have been calculated analytically²³. According to those results, the elastic energy stored in a region around the disk centre of size R_d —of the order of the spatial extent of a dislocation dipole—is roughly equal to $(R_d IB / 4\pi ch)^2 \pi / (4c_{66})$, where $B = \Phi_0 n$ is the average magnetic induction and n the areal density of flux lines. This energy is

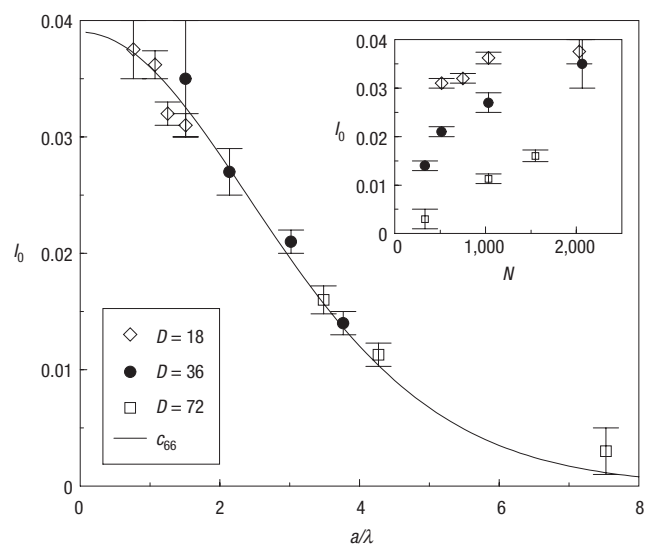


Figure 5 The threshold current I_0 . Inset: the value of I_0 as a function of the number of vortices N for different disk radii D . When plotted as a function of the lattice spacing a , the data collapse into a single curve, which follows the decay of c_{66} (main plot).

released by the formation of new dislocation pairs. On balancing the core energy with the elastic energy provided by the external current one can estimate the transition current

$$I_0 = \frac{4\sqrt{2}chbc_{66}}{R_d B} = \frac{4\sqrt{2}chb\Phi_0}{R_d(8\pi\lambda)^2} \frac{c_{66}}{\tilde{c}_{66}}, \quad (1)$$

where $\tilde{c}_{66} = B\Phi_0/(8\pi\lambda)^2$ is the long wavelength shear modulus in the continuum limit. In the units of current used in the simulations, this transition current is equal to $I_0 = 2^{1/2}b/(4\pi R_d)c_{66}/\tilde{c}_{66}$.

The vortex lattice is often considered as a conventional continuum elastic medium characterized by its compressional c_{11} , shear c_{66} , and tilt c_{44} moduli, disregarding its discrete nature. In the limit of very long wavelength distortions, however, the elastic properties are governed by local elastic moduli, which strongly depend on the strength of the magnetic field. Analytical results for the local compressional, shear, and tilt moduli of a discrete vortex lattice as a function of the lattice spacing a are provided elsewhere²⁹.

We compute systematically the variation of I_0 with N and D (see the inset of Fig. 5). When plotted as a function of the lattice spacing $a \equiv (2\pi D^2/3^{1/2}N)^{1/2}$, the scattered data can be collapsed into a single curve (Fig. 5, main plot) which follows the theoretical curve²⁹ c_{66}/\tilde{c}_{66} . When multiplied by an overall constant $C = 0.039 \pm 0.003$ the curve provides a good fit of the data. This constant is also in reasonably good agreement with its theoretical estimate $C = 2^{1/2}b/(4\pi R_d)$ (where $b = a$ and the dipole extent $R_d \approx 2-3a$).

In conclusion, we have shown that the onset of plastic flow in a superconducting disk occurs in close correspondence with the nucleation and motion of new dislocations in the vortex lattice. Once formed, dislocations glide parallel to their Burgers vector, releasing the shear stress concentration. On increasing the nucleation rate, dislocations arrange themselves into densely packed radial grain boundaries that cross the entire disk and tend to glide in a cooperative manner. The plastic response is characterized by a non-linear I - V curve and by strong fluctuations. These results have been obtained for a

two-dimensional geometry, and they could change when the thickness of the film is large. Our approach should be relevant, however, for thin films of other self-assembled nanostructures subject to the action of shearing forces^{1–3}, and possibly for granular media³². Obviously, the precise value of the driving force thresholds, signalling the onset of a nonlinear response and the plastic deformation of the sample, would depend on the appropriate physical parameters characterizing the interaction among the constituent elements in each case.

METHODS

We consider a set of N rigid vortices confined in a disk of radius D . The equation of motion for each vortex i at position \vec{r}_i

$$\Gamma \frac{d\vec{r}_i}{dt} = \sum_j \vec{f}_{VV}(\vec{r}_i - \vec{r}_j) + \vec{f}_L(\vec{r}_i), \quad (2)$$

where Γ is an effective viscosity. We choose as units of space and time λ and $t_0 = \Gamma\lambda/A$ respectively, and we measure the current I in units of $\Phi_0/(2\pi ch\lambda A)$. The N vortices are confined inside the disk by the external magnetic field and the sample edge barrier that we model by imposing an extra normal force on the vortices of the form $\vec{f}_B = -g \exp[-(D-r)/r_0] / r_0 \hat{r}$, with $r_0 = 0.1\lambda$ and $g/A = 1$. A similar force is also imposed at the inner wall close to the disk centre (at $r = r_0$), thus avoiding the singularity of the Lorentz force at $r = 0$.

The coupled equations (2) for $i = 1, \dots, N$ are integrated numerically with an adaptive step size fifth-order Runge–Kutta method with precision 10^{-6} . We do not truncate the range of the vortex–vortex interaction because this leads to spurious fluctuations caused by the force discontinuities. We study the response of the system as a function of the applied current for different values of N , ranging from $N = 332$ to $N = 2064$, and D ($D = 18\lambda, 36\lambda, 72\lambda$).

Received 29 January 2003; accepted 28 April 2003; published 22 June 2003.

References

- Murray, C., Kagan, C. & Bawendi, M. Synthesis and characterization of monodisperse nanocrystals and close-packed nanocrystal assemblies. *Annu. Rev. Mater. Sci.* **30**, 545–610 (2000).
- Mitchell, T. B., Bollinger, J. J., Itano, W. M. & Dubin, D. H. E. Stick slip dynamics of a stressed ion crystal. *Phys. Rev. Lett.* **87**, 183001 (2001).
- Pertsinidis, A. & Ling, X. S. Diffusion of point defects in two-dimensional colloidal crystals. *Nature* **413**, 47–50 (2001).
- Brandt, E. H. The flux-line lattice in type two superconductors. *Rep. Prog. Phys.* **58**, 1465–1594 (1995).
- Abrikosov, A. A. On the magnetic properties of superconductors of the second kind. *Sov. Phys. JETP* **5**, 1174–1182 (1957).
- Safar, H. *et al.* Experimental evidence for a first-order vortex-lattice-melting transition in untwinned, single crystal $\text{YBa}_2\text{Cu}_3\text{O}_7$. *Phys. Rev. Lett.* **69**, 824–827 (1992).
- Avraham, N. *et al.* Inverse melting of a vortex lattice. *Nature* **411**, 451–454 (2001).
- Bouquet, F. *et al.* An unusual phase transition to a second liquid vortex phase in the superconductor $\text{YBa}_2\text{Cu}_3\text{O}_7$. *Nature* **411**, 448–451 (2001).
- Schilling, A., Welp, U., Kwok, W. K. & Crabtree, G. W. Vortex-lattice melting in untwinned $\text{YBa}_2\text{Cu}_3\text{O}_{7-x}$ for $H \perp c$. *Phys. Rev. B* **65**, 054505 (2002).
- Fisher, D. S., Fisher, M. P. A. & Huse, D. Thermal fluctuations, quenched disorder, phase transitions, and transport in type II superconductors. *Phys. Rev. B* **43**, 130–159 (1991).
- Nelson, D. R. & Vinokur, V. M. Bose glass scaling for superconducting vortex arrays revisited. *Phys. Rev. B* **61**, 5917–5919 (2000).
- Giamarchi, T. & Le Doussal, P. Elastic theory of flux lattices in the presence of weak disorder. *Phys. Rev. B* **52**, 1242–1270 (1995).
- Klein, T. *et al.* A Bragg glass phase in the vortex lattice of a type II superconductor. *Nature* **413**, 404–406 (2001).
- Giamarchi, T. & Le Doussal, P. Moving glass theory of driven lattices with disorder. *Phys. Rev. B* **57**, 11356–11403 (1998).
- Crabtree, G. W., Lopez, D., Kwok, W. K., Safar, H. & Paulius, L. M. Dynamic correlation in driven vortex phases. *J. Low Temp. Phys.* **117**, 1313–1322 (1999).
- Bhattacharya, S. & Higgins, M. J. Dynamics of a disordered flux line lattice. *Phys. Rev. Lett.* **70**, 2617–2620 (1993).
- Marchevsky, M., Aarts, J., Kes, P. H., & Indenbom, M. V. Observation of the correlated vortex flow in NbSe_2 with magnetic decoration. *Phys. Rev. Lett.* **78**, 531–534 (1997).
- Paltiel, Y. *et al.* Dynamic instabilities and memory effects in vortex matter. *Nature* **403**, 398–401 (2000).
- Paltiel, Y. *et al.* Instabilities and disorder-driven first-order transition of the vortex lattice. *Phys. Rev. Lett.* **85**, 3712–3715 (2000).
- D’Anna, G. *et al.* Evidence of surface superconductivity in 2H-NbSe₂ single crystals. *Phys. Rev. B* **54**, 6583–6586 (1996).
- López, D. *et al.* Spatially resolved dynamic correlation in the vortex state of high temperature superconductors. *Phys. Rev. Lett.* **82**, 1277–1280 (1999).
- Marchetti, M. C. & Nelson, D. R. Vortex physics in confined geometries. *Physica C* **330**, 105–129 (2000).
- Benetatos, P. & Marchetti, M. C. Plasticity in current-driven vortex lattices. *Phys. Rev. B* **65**, 134517 (2002).
- Jensen, H. J., Brass, A. & Berlinsky, A. J. Lattice deformations and plastic flow through bottlenecks in a two-dimensional model for flux pinning in type-II superconductors. *Phys. Rev. Lett.* **60**, 1676–1679 (1988).
- Fangohr, H., Cox, S. J. & de Groot, P. A. J. Vortex dynamics in two-dimensional systems at high driving forces. *Phys. Rev. B* **64**, 064505 (2001).
- Chen, Q.-H. & Hu, X. Nonequilibrium phase transitions of vortex matter in three-dimensional layered superconductors. *Phys. Rev. Lett.* **90**, 117005 (2003).
- Miguel, M.-C., Vespignani, A., Zapperi, S., Weiss, J. & Grasso, J. R. Intermittent dislocation flow in viscoplastic deformation. *Nature* **410**, 667–671 (2001).
- Hirth, J. P. & Lothe, J. *Theory of Dislocations* (Krieger, Malabar, Florida, 1992).
- Miguel, M.-C. & Kardar, M. Elasticity and melting of vortex crystals in anisotropic superconductors: Beyond the continuum regime. *Phys. Rev. B* **62**, 5942–5956 (2000).
- de Gennes, P.-G. *Superconductivity of Metals and Alloys* (Benjamin, New York, 1966).
- Chaikin, P. M. & Lubensky, T. C. *Principles of Condensed Matter Physics* (Cambridge Univ. Press, Cambridge, 1995).
- Veje, C. T., Howell, D. W. & Behringer, R. P. Kinematics of a two-dimensional granular Couette experiment at the transition to shearing. *Phys. Rev. E* **59**, 739–745 (1999).

Acknowledgements

We thank G. Jung, M. Zaiser, R. Pastor-Satorras, and J. S. Andrade Jr. for useful remarks. This work is supported by an Italy–Spain Integrated Action. M.C.M. is supported by the Ministerio de Ciencia y Tecnología (Spain).

Correspondance and requests for materials should be addressed to S.Z.

Supplementary Information accompanies the paper on www.nature.com/naturematerials

Competing financial interests

The authors declare that they have no competing financial interests.

SUPPLEMENTARY MOVIE CAPTIONS:

These animations show the evolution of the Delaunay triangulation for different parameter values. Each snapshot is separated by $dt = 10$ timesteps and the sequence is cycled. Five-fold vortices are shown in red and seven-fold vortices in green.

1. The onset of plastic flow ($I=0.04$) in a system of radius $D = 18$ with $N = 1032$ vortices.
2. The onset of plastic flow ($I = 0.04$) in a system of radius $D = 36$ with $N = 1032$ vortices.
3. The laminar phase ($I = 0.3$) when defects are arranged into grain boundaries, in a system of radius $D = 18$ with $N = 1-32$ vortices.
4. The laminar phase ($I = 0.3$) when defects are arranged into grain boundaries, in a system of radius $D = 36$ with $N = 2064$ vortices.
5. The first transient steps before reaching the laminar phase corresponding ($I = 0.3$) in a system of radius $D = 36$ with $N = 2064$ vortices. In this animation each snapshot is separated by $dt = 3$ timesteps and the sequence is cycled.

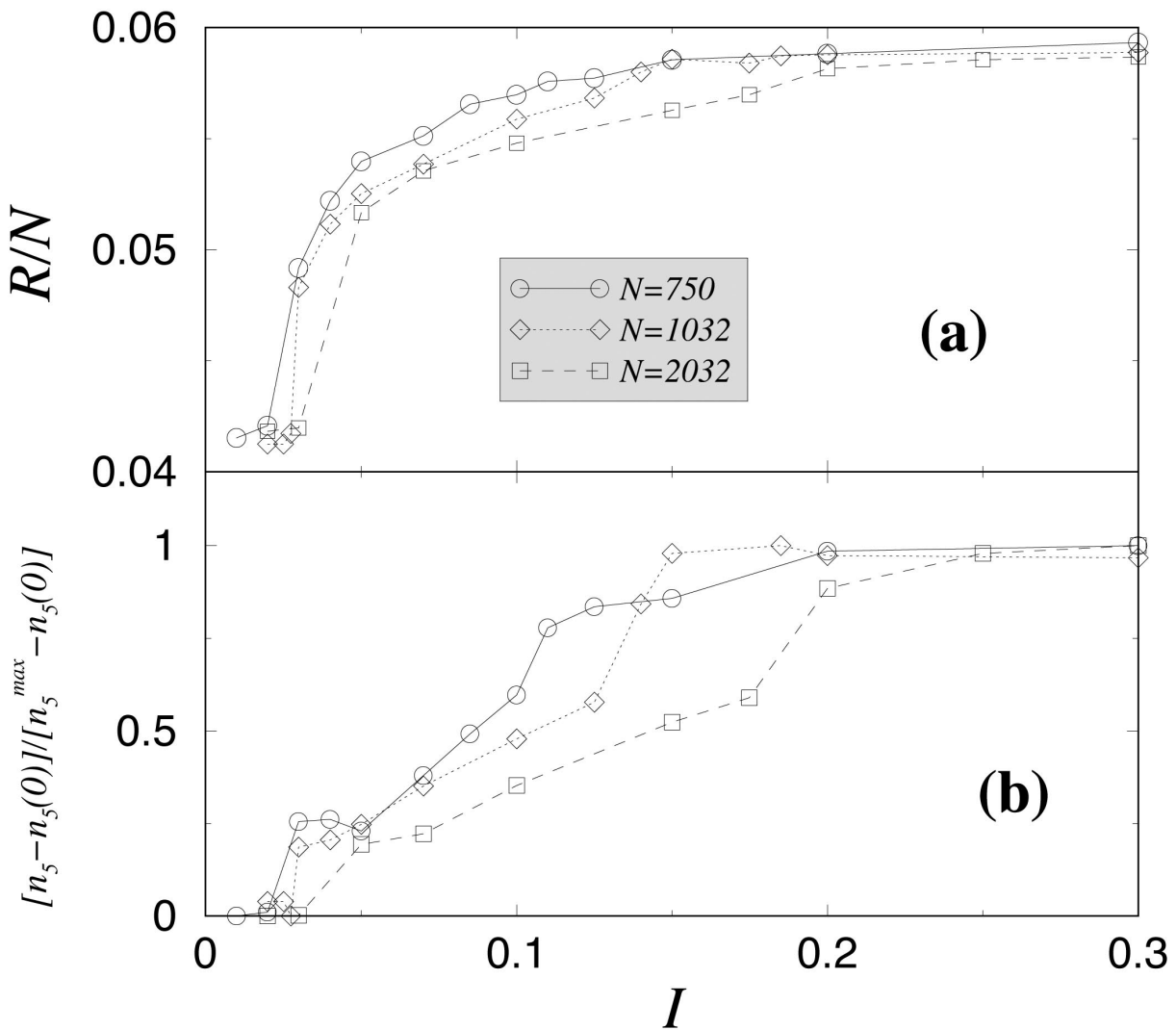


FIGURE 1

(a) The resistance R/N as a function of the applied current for N vortices in a disk of radius $D = 36$. (b) The excursions in the average steady number of five-fold coordinated vortices n_5 for different N is shown plotting $(n_5 - n_5(0)) / (n_5^{\max} - n_5(0))$.

SUPPLEMENTARY INFORMATION

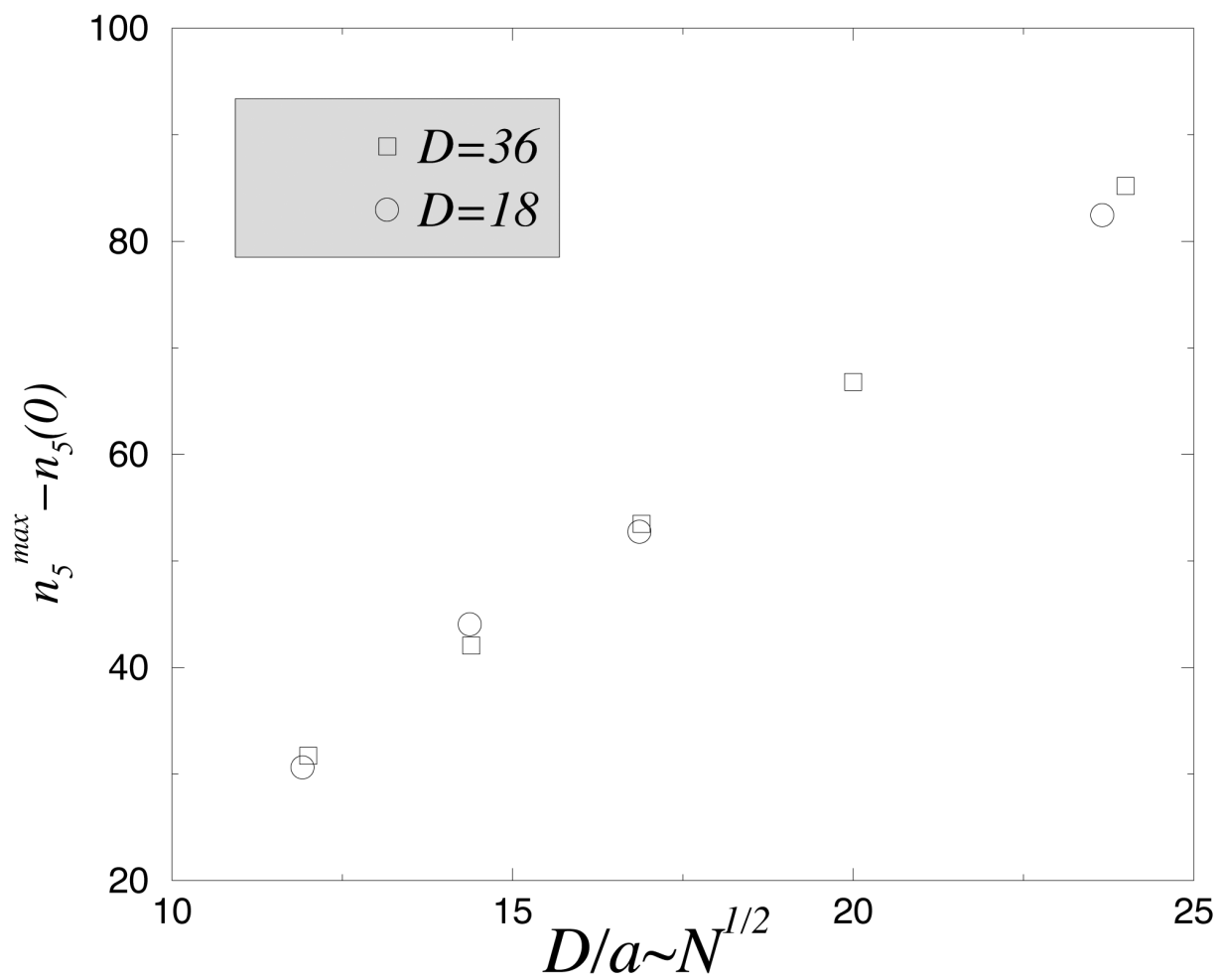


FIGURE 2 The plot shows that the asymptotic value ($n_5^{\max} - n_5(0)$) is a linear function of D/a , in close correspondence with the number of dislocations that fit into densely packed grain boundaries of size D .